One-Pot Synthesis of Reduced Graphene Oxide/Metal

(Oxide) Composites

Xu Wu, Yuqian Xing, David Pierce, Julia Xiaojun Zhao*

Department of Chemistry, University of North Dakota, Grand Forks, ND 58202, USA

KEYWORDS: Reduced graphene oxide, gold nanoparticles, copper(I) oxide nanoparticles, silver nanoparticles, hybrid compostie, electrocatalysis, electrochemical analysis, glucose.

ABSTRACT: Graphene, one of the most attracting two-dimensional nanomaterials, has demonstrated a broad range of applications because of its excellent electronic, mechanical, optical and chemical properties. In this work a general, environmental-friendly, one-pot method for the fabrication of reduced graphene oxide (RGO)/metal (oxide) (e.g. RGO/Au, RGO/Cu₂O, and RGO/Ag) composties was developed using glucose as the reducing agent and the stabilizer. The glucose not only reduced GO effectively to RGO, but also reduced the metal precursors to form metal (oxide) nanoparticles on the surface of RGO. Moreover, the RGO/metal (oxide) composites were stabilized by gluconic acid on the surface of RGO. The developed RGO/metal (oxide) composites were characterized using STEM, FE-SEM, EDS, UV-vis absorption spectroscopy, XRD, FT-IR and Raman spectroscopy. Finally, the developed nanomaterials were successfully applied as an electrode catalyst to simultaneous electrochemical analysis of L-ascorbic acid (L-AA), dopamine (DA) and uric acid.

1. Introduction

Graphene, a two-dimensional carbon nanomaterial containing a monolayer of sp^2 hybridized carbon atoms, has attracted increasing attention due to its useful electronic, thermal, and optical properties.¹⁻⁷ Graphene is usually synthesized by the modified Hummer's method, which forms graphene oxide (GO) from graphite with ultrasonication, afterwards, oxygen-containing groups on the GO are treated to form reduced graphene oxide (RGO). The electrical and thermal conductivity of RGO exceeds those of GO even though they are still lower than pristine graphene. 8-10 However, the residual oxygen-containing groups in RGO (carboxyl, epoxy, carbonyl, and hydroxyl) provide active sites for further chemical modification and decoration with other nanomaterials, thereby allowing electronic and optoelectronic properties to be tailored. 11-12 When modified with inorganic nanomaterials (e.g., Au, Cu, Ag, TiO₂, Fe₃O₄, QDs, SiO₂, and etc.), graphene has found numerous applications in fields such as solar energy storage, ¹³ Li-ion battery fabrication, 14 biosensors, 15 and drug delivery. 16-17 For instance, Xu et al. adsorbed metal nanoparticles (Au, Pt and Pd nanoparticles) on the surface of GO followed by reduction of GO to RGO using ethylene glycol. 18 The resulting graphene-Pt composites showed promise in direct methanol fuel cells. Sun's group developed a series of methods for decorating inorganic nanoparticles on the surface of reduced graphene oxide and expanded their applications in the field of bioanalysis and electrocatalysts. 19-30 Lightcap et al. anchored semiconductor and metal nanoparticles on RGO at separate sites.³¹ With UV irradiation, the photogenerated electrons from TiO₂ were captured and transferred through RGO to reduce silver ions to silver nanoparticles apart from TiO₂. This electron storage and shuttling ability of RGO demonstrated its potential use as a catalytic nanocomposite.

In general, there are two different pathways to fabricate graphene-inorganic nanocomposites including *ex situ* hybridization and *in situ* decoration.⁷ In the process of *ex situ* hybridization, the inorganic nanoparticles are synthesized separately from graphene using traditional methods. Afterwards, the well-defined inorganic nanoparticles are adsorbed onto the surface of RGO through either covalent or non-covalent binding. This method ensures better shape and size control of the inorganic nanoparticles.³² Meanwhile, surface modification of inorganic nanoparticles can be easily conducted prior to their hybridization

with RGO. However, all the inorganic nanoparticles should be prepared in advance for *ex situ* hybridization, which complicates the preparation process. Also, loading efficiency of the inorganic nanoparticles on RGO is usually lower than *in situ* methods.³³ Accordingly, *in situ* methods for the fabrication of RGO-inorganic nanocomposites have received increasing attention.³⁴⁻³⁵

Several inorganic nanoparticles, especially metallic nanoparticles have been decorated on the surface of GO or RGO using *in situ* methods.³⁶⁻³⁸ Usually, the metal precursors are added directly to the graphene materials for a one-pot synthetic method that dramatically simplifies the synthetic process. The oxygencontaining groups in GO and RGO provide nucleation sites for crystallization of the metal nanoparticles.¹¹⁻¹² Meanwhile, with the introduction of reducing agents, the metal precursors and GO could be simultaneously reduced in solution.³⁹ However, two main limitations of these *in situ* methods are (i) the unstable dispersion of RGO in aqueous solutions due to the removal of oxygen-containing groups and (ii) the use of toxic reducing agents (e.g., hydrazine and sodium borohydride). To improve stability of the RGO-inorganic nanocomposites, surfactants and polymers can be adsorbed to the surface of RGO prior to the reducing process.⁴⁰⁻⁴² To avoid toxic reducing agents, biocompatible reagents, such as ascorbic acid,³⁹ glucose,⁴³ sodium citrate⁴⁴ and ethylene glycol,⁴⁵ can be used to reduce GO and metal precursors. However, in most of these methods, an extra stabilizer, such as sodium dodecyl sulfate (SDS), is usually needed to disperse the resulting RGO-inorganic nanocomposites in solution.⁴⁶ Therefore, a general simple *in situ* method to decorate RGO with inorganic nanocomposites is needed.

The present work demonstrates a generalized, environmental-friendly *in situ* method for fabrication of RGO-metal (oxide) composite materials. The environmentally benign reagent, glucose, was found to be an especially effective reductant and solution stabilizer in the one-pot synthetic process. Moreover, the process was found to be adaptable for synthesizing a variety of RGO/metal (oxide) composites, including RGO/Au, RGO/Cu₂O and RGO/Ag. Extensive characterizations were used to confirm the composition and morphology of the designed composites. Furthermore, the electrocatalytic activity of the RGO/Au nanocomposite was demonstrated.

L-AA, DA and UA play important roles in physiological processes of the human metabolism. 47-48 Several disease states and disorders can be monitored by measuring the levels of these biomolecules under physiological conditions. 49-51 For instance, DA is an important neurotransmitter in the mammalian central nervous system but usually present very low concentration (0.01-1 µM). However, L-AA and UA usually coexist in the extra cellular fluid of the central nervous system and serum but the concentrations were more than 100 times higher than DA.⁵² Especially, oxidation peaks of these three biomolecules occur at similar potentials, often resulting in an undistinguishable overlap when they are detected simultaneously. Modification of carbon electrodes with nitrogen-doped graphene, chitosan, carbon nanotube and gold nanoparticles improves the electrochemical oxidation of these three biomolecules and has provided a reliable means for their simultaneous detection. 53-57 This improved performance has been especially true for a variety of recently developed gold nanomaterials. However, by coupling RGO with gold nanoparticles, the electrochemical analytical performance might be improved because of the large surface area and high conductivity of RGO. Meanwhile, RGO could provide a platform for gold nanoparticles to anchor on the surface of electrode without other assistant molecules, like chitosan. By simultaneous analysis of L-ascorbic acid (L-AA), dopamine (DA) and uric acid (UA) under physiological solution conditions, the results illustrated the potential of the developed composites for other biomolecule detection schemes.

2. Experimental Section

2.1 Materials. Graphene oxide was purchased from Cheap Tubes Inc., VT. Glucose (≥99.5%, GC grade), L-ascorbic acid (L-AA, ≥99.0%, crystalline), dopamine hydrochloride (DA), uric acid (UA, ≥99%, crystalline), chloroaunic acid tetrahydrate (+99.9%), copper(II) chloride dehydrate (ACS reagent, ≥99.0%), silver nitrate (ACS reagent, ≥99.0%) and ammonium hydroxide (ACS reagent, 28.0%) were purchased from Sigma Aldrich Inc. Phosphate buffered saline tablets and fetal bovine serum were purchased from Fisher Scientific. Deionized (DI) water (Millipore Milli-Q grade) with resistivity of 18.2 MΩ•cm was used in all experiments.

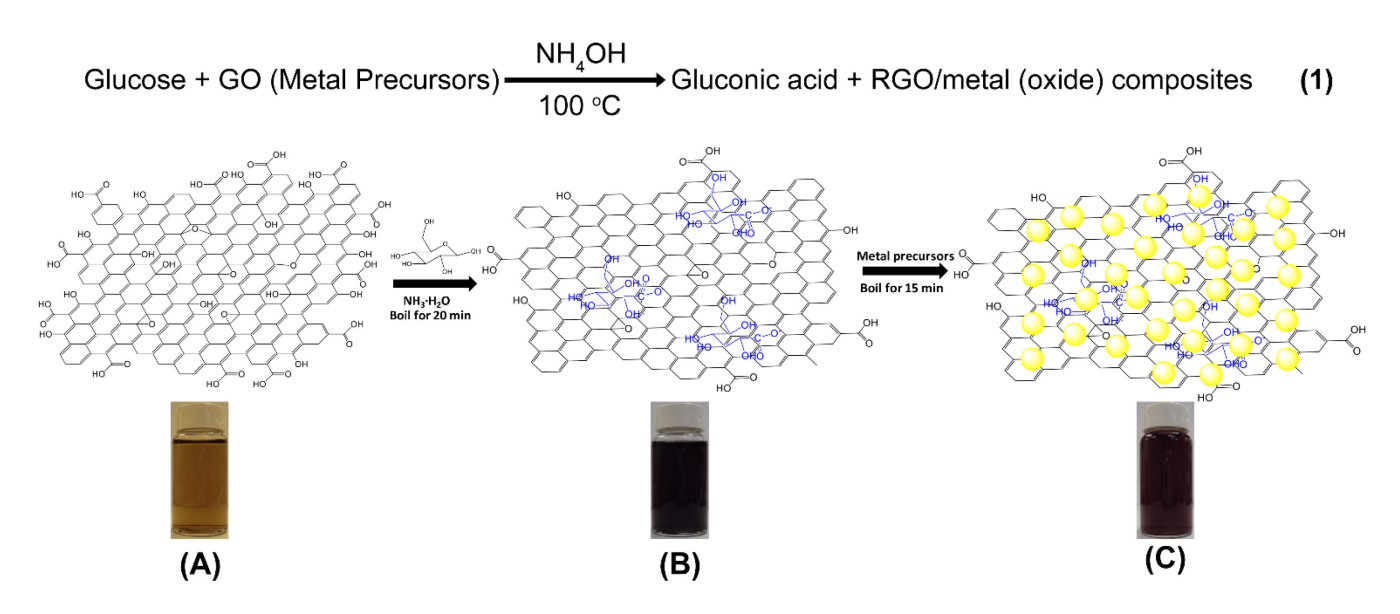
- 2.2 Preparation of RGO/Metal (Oxide) Composites. The RGO/metal (oxide) composites were prepared using a one-pot reaction. In brief, 160.0 mg glucose was added to a stirred homogeneous GO solution (100.0 mL, 5.0 mg) and stirred for 30 min. An 80 μL aliquot of NH₄OH (29.0 %) was added quickly to the solution and the flask was heated to boiling for 20 min. During this time, the color of the solution changed from brown-yellow to dark black, indicating the formation of RGO from GO. Afterwards, 1.0 mL of the metal precursor solution (1.0 % HAuCl₄, 1.0 % CuCl₂ or 0.5 % AgNO₃) was added drop wise and the mixture was boiled for 15 min. Finally, the cooled dispersed solution was centrifuged at 7000 rpm for 30 min to separate the unattached metal nanoparticles that remained suspended in the supernatant during the centrifugation. The RGO/metal composite precipitate was redispersed into 20.0 mL Milli-Q water with sonication for further usage.
- 2.3 Characterization. The scanning transmission electron microscopy (STEM) and scanning electron microscopy (SEM) images of RGO/metal (oxide) composites were obtained with a Hitachi SU8010 field emission scanning electron microscope. The diameters of the metal(oxide) particles were measured using Image J, at least 50 different nanoparticles for each sample were measured. Elemental analysis for different RGO/metal composites was performed by an energy-dispersive X-ray spectroscope (EDS) (Oxford, X-Max) installed in the Hitachi SU8010 SEM. TEM and HRTEM images were taken with FEI Tecnai F20 (200 kV). X-ray diffraction (XRD) profiles were obtained with a Bruker AXS D8 advanced powder X-ray diffraction system using Cu Kα radiation. Raman spectra were obtained with an Aramis labRAM Raman spectrometer (Horiba JobinYvon) using a helium-neon laser at 542 nm. Fourier transform infrared (FTIR) spectra were obtained with a FT-IR spectrometer (Spectrum 400, PekinElmer) and UV-vis absorption spectra were recorded with a Shimadzu UV-250 spectrometer.
- **2.4 Electrochemical Measurement.** All cyclic voltammetry (CV) and differential pulse voltammetry (DPV) were performed with an Autolab PGSTAT302 potentiostat using a standard three-electrode cell. The cell was configured in all experiments with a Ag/AgCl (saturated KCl) reference electrode, a platinum wire counter electrode, and a modified glassy carbon electrode (GCE, 5 mm diameter, BASi). Prior to the

medication, the GCE was cleaned by polishing with an aqueous suspension of 0.05 mm alumina powders (Buehler), rinsing with DI water under sonication and then electrochemical cycling in 1.0 M H₂SO₄ from - 0.4 V to 1.5 V until a stable CV was obtained. After rinsing and drying the cleaned electrode, a 20 μL aliquot of GO, RGO or RGO/Au nanocomposites was drop-cast onto the GCE surface and dried in a 60°C oven for 30 min.

CV and DPV measurements of L-AA, DA and UA were performed at room temperature with a 0.01 M pH 7.0 PBS buffer and usually containing 10-times diluted serum to model physiological conditions. The DPV analysis was conducted with L-AA, DA and UA stock solutions spiked into the PBS buffer with a diluted serum.

3. Results and Discussion

3.1 Design and Synthesis of the RGO/Metal (Oxide) Composites. The designed one-pot synthetic process for RGO/metal (oxide) composite was shown in Scheme 1. This method has three main features. First, the reductant used in the synthetic process is environmental friendly, by being natural and non-toxic. Secondly, the reductant plays multiple roles in the synthetic process as a reductant for both GO and metal precursors and as a stabilizer for protection of the product from aggregation. Thirdly, this synthetic method is general enough to produce different types of RGO/metal (oxide) composites. The rational of selection of glucose as the reductant is based on its natural and nontoxic properties as well as its abundance and relatively gentle activity. Other natural substances, such as sucrose, fructose and L-ascorbic acid, have also been used for the reduction process. 43, 58 However, glucose has already been proven to be useful for the reduction of GO.⁴³ After reducing GO, glucose is oxidized to gluconic acid that was used as a stabilizer to remain RGO stable in aqueous solution. 43 Meanwhile, glucose has been used for the synthesis of gold and silver nanoparticles.⁵⁹ However, no report was presented to prepare RGO/metal composite using glucose as an environmental-friendly reducing agent. Inspired by these works, we developed the one-pot approach for the synthesis of RGO/metal (oxide) composites using glucose as the multifunctional reducing agent and stabilizer precursor as shown in Scheme 1. This strategy not only provided a universal pathway to produce stable RGO-based composite for different applications, but also eliminated the utility of toxic materials in the synthesis process.



Scheme 1. Illustration of the synthetic process of RGO/metal (oxide) composites using glucose as the reducing agent. (A) GO was stirred with glucose without heating; (B) GO was reduced to form RGO by glucose with boiling for 20 min; (C) RGO/metal(oxide) composites were formed through the injection of metal precursors in (B) for boiling another 15 min.

In Scheme 1, the oxygen-containing groups on GO, such as carboxyl and hydroxyl groups, were removed under thermal treatment with an excess of glucose as the reducing agent. The color of the solution changed from brown-yellow (Scheme 1A) to dark black (Scheme 1B) indicated the formation of the RGO from GO. In literatures, RGO was reduced by other methods, including thermal treatment and chemical reduction, which suffered from unstable suspension because most of the oxygen-containing groups were removed from GO and electrostatic repulsion between the RGO sheets decreased significantly. In contrast, RGO reduced by glucose was more stable in water suspension due to the protection of gluconic acid on the surface of RGO. Moreover, the gluconic acid and residual oxygen groups on RGOs provided reactive sites for absorption and nucleation of different metal ions onto the surface of RGO, followed by reduction of metal ions to form the nanoparticles on these sites (Scheme 1C). The color of the solution changed with

the addition of metal precursors, indicating the formation of different metal (oxide) nanoparticles on the surface of RGOs. The resulted RGO/metal (oxide) composites required several centrifugation/washing cycles with DI water to ensure separation of dispersed metal nanoparticles from the nanoparticle-decorated RGOs.

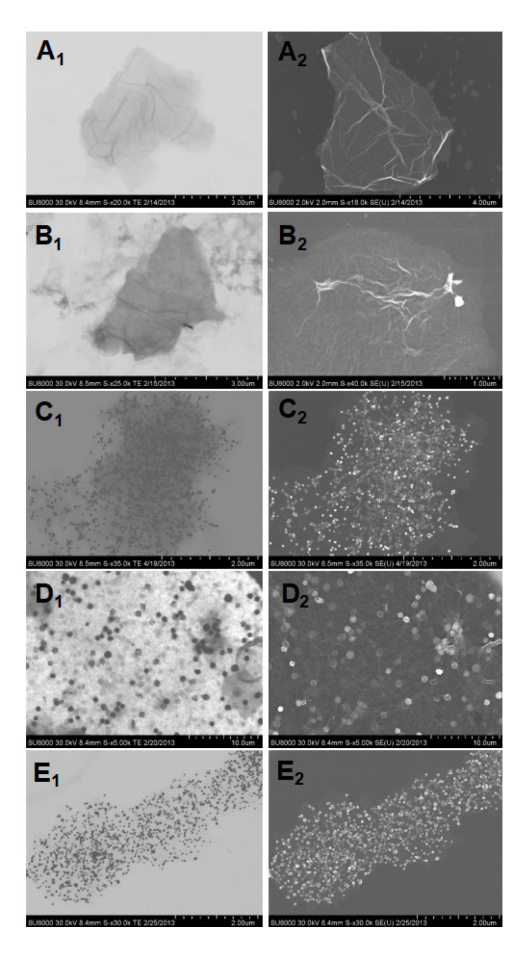


Figure 1. The STEM (A1, B1, C1, D1 and E1) and FE-SEM (A2, B2, C2, C2, D2 and E2) images of GO (A1 and A2), RGO (B1 and B2), RGO/Au (C1 and C2), RGO/Ag (D1 and D2) and RGO/Cu2O (E1 and E2) nanocomposites. Reaction conditions: 100.0 mL of GO solution, 160.0 mg of glucose, and 80 μL of NH4OH were mixed to form a homogenous solution. The solution was boiled for 20 min followed by the addition of 1.0 mL metal precursors for another 15 min of boiling.

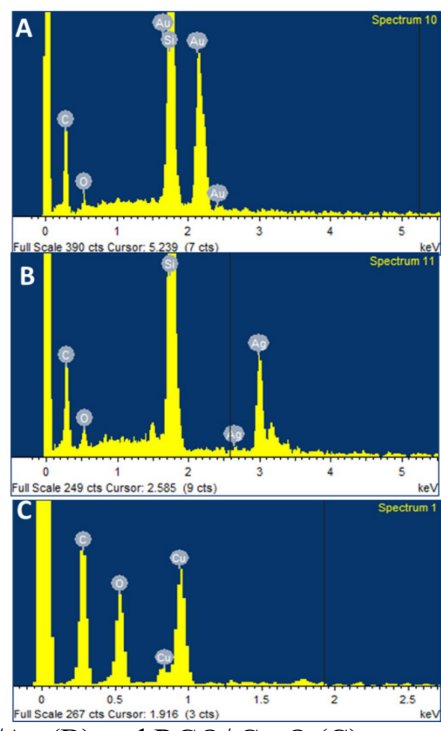


Figure 2. EDS of RGO/Au (A), RGO/Ag (B) and RGO/Cu₂O (C) nanocomposites. Reaction conditions: The mixture of 100.0 mL of GO solution, 160.0 mg of glucose, 80.0 μL of NH₄OH was boiling for 20 min followed by the addition of 1.0 mL of different metal precursors for another 15 min.

3.2 Characterization of Designed Composites. Composites were characterized with a number of methods including imaging, elemental analysis, and spectroscopies. The following results confirmed our design.

3.2.1 Morphology and elemental analysis of the developed composites. Successful decoration of different metal (oxide) nanoparticles onto RGOs was demonstrated by STEM images (Figure 1, images of 1 series) and SEM images (Figure 1, images of 2 series). First, before the reaction, the pure GO was imaged (A₁ and A₂). The both STEM and SEM images clearly showed GO sheet structures. After the reaction with glucose, little difference can be observed (B₁ and B₂) compared to A1 and A1although spectroscopy results described in the next section confirmed the distinct oxidation state of RGO. When an addition of different metal precursors was added to the RGO, the images clearly showed metal or metal oxide nanoparticles formed on the RGO surface (Figure 1 C-E). Specifically, an addition of HAuCl4

yielded 45.3 ± 0.8 nm gold nanoparticles which fully coated RGO (Figure 1 C₁ and C₂). The energy dispersive X-ray (EDS) analysis of this sample indicated that the nanoparticles were Au (Figure 2A). To test the universal potential of this phenomenon to other metal elements, an Ag precursor (AgNO₃) was added to the RGO solution. As expected, the RGO surface was successfully decorated with Ag nanoparticles (Figure 1 D₁ and D₂), and the EDS spectra indicted the presence of element of Ag (Figure 2B). Furthermore, we demonstrated the crystal structures of Au nanoparticles (Figure 3A and B) and Ag nanoparticles (Figure 3C and D) through the TEM and HRTEM images.

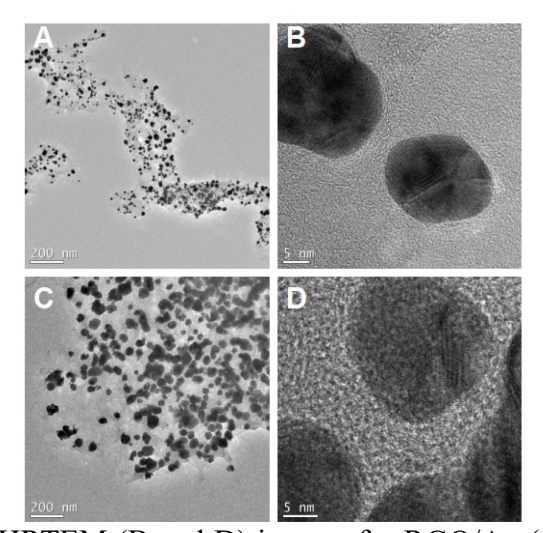


Figure 3. TEM (A and C) and HRTEM (B and D) images for RGO/Au (A and B) and RGO/Ag (C and D) nanocomposites.

In addition to the formation of pure metal nanoparticles, some metal oxide particles could be produced on the RGO surface. We treated RGO solution with a copper precursor (CuCl₂), The particles were produced (Figure 1 E₁ and E2). However, the elemental analysis (Figure 2C) of the particles was significantly distinct from Au and Ag. In Figure 2 C, the atomic ratio of carbon to oxygen was 1: 2.33, which was higher oxygen content than the other two nanoparticles formed from Au and Ag precursors (1: 2.11 and 1: 2.05 for RGO/Au and RGO/Ag, respectively), indicating the possible formation of copper (I) oxide particles instead of copper particles, because copper (II) was usually reduced to form brick red copper (I) by reducing sugar, such as Benedict's reagent and Fehling's solution.

SEM images showed that metal and metal oxide nanoparticles on each side of RGO could be easily distinguished based on their different contrasts. Wrinkles of the RGO could be recognized especially from the area with nanoparticles. It seems that the nanoparticles were trapped within the RGO sheet. Average diameters of these nanoparticles were statistically calculated from the measurements of multiple nanoparticles (N > 50). The results were 45.3 ± 0.8 nm (Au), 53.4 ± 0.9 nm (Ag) and 675.1 ± 9.2 nm (Cu₂O). Overall, the above results demonstrated that different metal (oxide) particles could be decorated on the surface of RGO during the *in situ* reduction process using glucose as a reductant.

3.2.2 Spectroscopic characterizations. We further confirmed the developed composites using UVvis spectra, FTIR, Raman spectra and XRD. First, we investigated their UV-vis spectra (Figure 4A). UVvis absorption spectrometry is a powerful tool to distinguish the GO from RGO since they were hard to be differentiated from the previous microscopic images. It should show a red shift on the absorption peak if GO becomes RGO according to the literature.³⁹ In our result, the pure GO showed a typical absorption peak at 230 nm (Figure 4A curve a). After 20 min of reaction with glucose, the 230 nm absorption peak was shifted to 260 nm (Figure 4A curve b). This peak shift was an indication of the change from GO to RGO. The formation of metal (oxide) nanoparticles on the RGO can also be confirmed from their UV-vis absorption spectra. After the reaction with the metal precursors, RGO remained its original absorption peak at 260 nm. Meanwhile, a second absorption peak appeared at 560 nm for Au (Figure 4A curve c), which was corresponded to the red color of the RGO/Au nanocomposite. Similar to the RGO/Au nanocomposite, an absorption peak at 425 nm was formed for Ag (Figure 4A curve e) which was assigned to the color of yellow. However, the copper-based composite showed no second absorption peak (Figure 4A) curve d) although the resulted RGO/Cu₂O composites appeared a light blue color in solution, which might be resulted from the large size of Cu₂O particles. The reduction of GO to RGO was further confirmed by other three spectroscopic methods below.

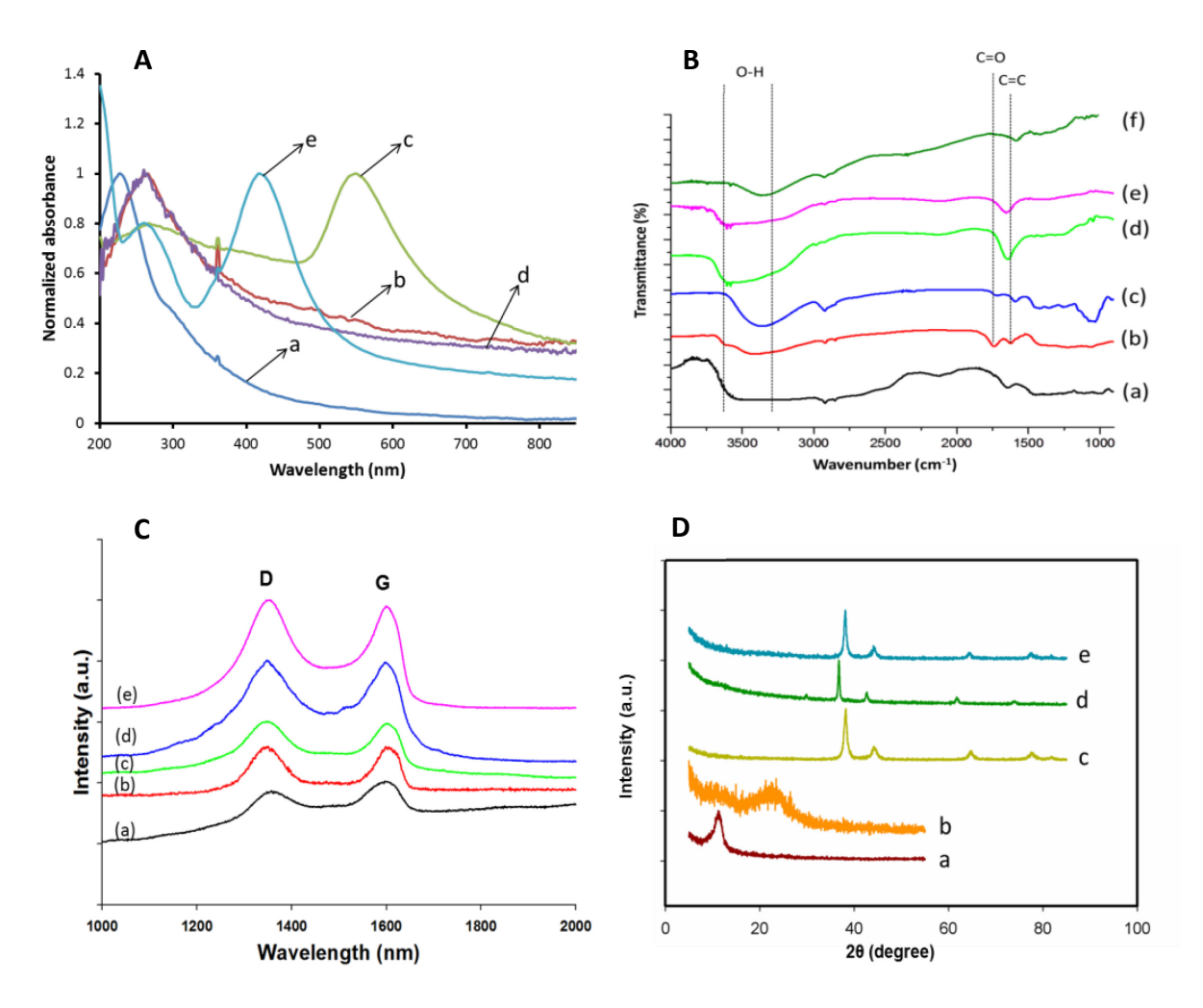


Figure 4. (A) Absorption spectra: GO (a), RGO (b), RGO/Au (c), RGO/Cu₂O (d) and RGO/Ag (e) nanocomposites. (B) FT-IR spectra of glucose (a), GO (b), RGO (c), RGO/ Cu₂O (d), RGO/Au (e) and RGO/Ag (f) nanocomposites. (C) Raman spectra of GO (a), RGO (b), RGO/Au (c), RGO/ Cu₂O (d) and RGO/Ag (e) nanocomposites. (D) XRD patterns of GO (a), RGO (b), RGO/Au (c), RGO/ Cu₂O (d) and RGO/Ag (e) nanocomposites. Reaction conditions: the mixture of 100.0 mL of GO solution, 160.0 mg of glucose, 80.0 μL of NH₄OH was boiling for 20 min followed by the addition of 1.0 mL of different metal precursors for another 15 min.

We then performed FT-IR spectrometry to further confirm the reduction of GO to RGO (Figure 4B). As a control, first, the pure glucose's FT-IR spectrum was recorded (Figure 4B curve a). Compared to the pure glucose, GO showed a strong infrared absorption band at 1725 cm⁻¹ due to C=O stretching (Figure 4B curve b). When the GO was reduced by glucose, this peak decreased significantly while the C=C

stretching peak at 1620 cm⁻¹ appeared (Figure 4B curve c). The peak shift from C=O to C=C indicated the reduction of GO to RGO. Furthermore, we tested Au, Ag and Cu₂O decorated RGO. As shown in Figure 4B curves d, e, and f, their FT-IR spectra clearly showed the C=C peak around 1620 cm⁻¹ but the C=O peak at 1725 cm⁻¹was not visible. The FT-IR spectrometry results supported the reduction of GO to RGO by glucose.

Raman spectra further demonstrated different structural signatures between GO and its reduced products by glucose (Figure 4C). In general, when GO is reduced to RGO, one of the typical structure changes is to form sp^2 domain structure. The change could be evidenced by the increased intensity ratio of the D band at 1350 cm⁻¹ to the G band at 1595 cm⁻¹ (I_D/I_G). As shown in Figure 3C, the ratio of I_D to I_G was 0.92 for the pure GO (Figure 4C curve a); however, the ratio was increased to 1.04 after the glucose was used to reduce the GO (Figure 4C curve b). The 13% increase in the ratio of I_D to I_G indicated the formation of RGO. We then tested the Au, Cu₂O and Ag nanoparticles decorated RGO (Figure 4C curve c, d and e). All these samples showed apparent D and G bands for which the ratios of I_D to I_G were 1.03, 1.08 and 1.03, respectively. These results demonstrated that GO had been reduced by glucose and formed a more sp^2 -like ordered structure.

Structures of GO, RGO, RGO/Au, RGO/Cu₂O and RGO/Ag composites were further characterized using powder XRD (Figure 4D). GO showed a graphitic diffraction peak at 11.5° (Figure 4D curve a), corresponding to an interlayer d-spacing of 0.73 nm. Compared to 0.34 nm of d-spacing of pristine graphite (0.34 nm)³⁷, the larger d-spacing distance indicated that the oxygenated functional groups were introduced into the carbon sheet. Then the peak at 11.5° disappeared and a bump around 20° formed for the newly formed RGO (Figure 4D curve b), which demonstrated the removal of the oxygen-containing groups from GO and exfoliation of the layered RGO. Once metal (oxide) nanoparticles were introduced on the surface of the RGO, their corresponding peaks were evident. For example, RGO/Au (Figure 4D curve c) showed the peaks at 38.4°, 44.2°, and 64.7° (matched with JCPDS: 01-1174) which can be assigned to (111), (200) and (220) faces of the Au nanoparticles. RGO/Cu₂O and RGO/Ag also showed

characteristic peaks at 29.5°, 36.3°, 42.5°, 61.5° (matched with JCPDS: 05-0667) and 38.1°, 42.2°, 64.5° and 77.5° (matched with JCPDS: 04-0783), respectively (Figure 4D curve d and e).

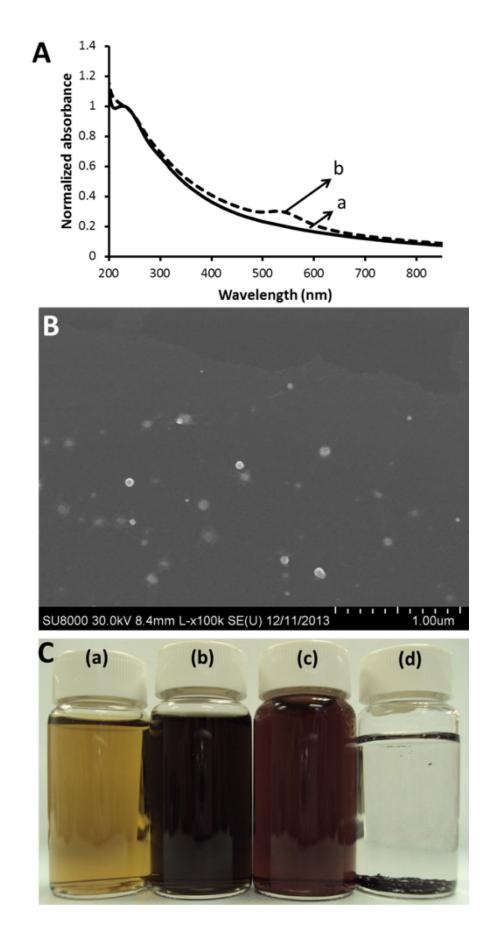


Figure 5. (A) Absorption spectra of GO (curve a) and GO/Au nanocomposite (curve b) without glucose addition. (B) SEM images of the GO/Au nanocomposites without addition of glucose. (C) Photographs of aqueous dispersions of 0.05 mg/mL GO (a), RGO reduced by glucose (b), RGO/Au nanocomposites (c) and RGO reduced by the hydrazine hydrate (d). Solution (a), (b) and (c) were stored for about 3 months. Solution (d) was stored for 1 day.

The above characterization results have confirmed our design that the GO has been reduced to RGO and then different types of metal (oxide) nanoparticles decorated on the surface of the produced RGO. Afterwards, we optimized the synthetic conditions for making RGO/metal (oxide) composites. RGO/Au nanocomposite was chosen as an example for this optimization.

3.3 Optimization of Composite Synthesis. Various experimental conditions would affect the formation of RGO/Au nanocomposites. Here, we investigated a few important conditions that may play crucial roles for the formation of the designed composites.

3.3.1 Effect of glucose. As the solo reductant and stabilizer, glucose played an important role in the synthesis. Therefore, we investigate the effect of glucose on the formation of composite. First, glucose acted as a reductant for the generation of both gold nanoparticles and RGO. Thereafter, glucose served as a stabilizer for RGO and RGO/Au nanocomposite. We repeated the synthetic process without addition of any glucose to observe the resulted product. It was found that the absorption peak of GO at 230 nm still existed in either solution before (Figure 5A, curve a) and after (Figure 5A, curve b) the addition of HAuCl4. However, there was no peak appeared at 260 nm which attributed to RGO. This implied that GO was not reduced without the addition of glucose. Interestingly, after the addition of HAuCl4, red colored gold nanoparticles were still formed, with the absorption peak at 538 nm (Figure 5A, curve b). SEM image showed that all the gold nanoparticles were anchored to the surface of GO (Figure 5B). However, compared with Figure 1C₁ and C₂, less gold nanoparticles were coated on to the surface of GO, which might be due to the loss of glucose on GO.

We then studied the function of glucose as a stabilizer to protect RGO from aggregation. As shown in Figure 5C, GO, RGO and RGO/Au nanocomposite reduced by glucose were stable in aqueous solution for more than 3 months (Figure 5 C, a, b and c). Usually, GO was reduced by the strong reductant, such as hydrazine hydrate. However, the instability of RGO reduced by hydrazine hydrate limited their applications in analysis. Therefore, we synthesized RGO using hydrazine hydrate as a control. The result showed that the RGO reduced by hydrazine hydrate was not stable. It started aggregation quickly. As shown in Figure 5C, (d), the RGO totally precipitated in one day. This is significantly different than that three month-stable RGO obtained using glucose as a stabilizer.

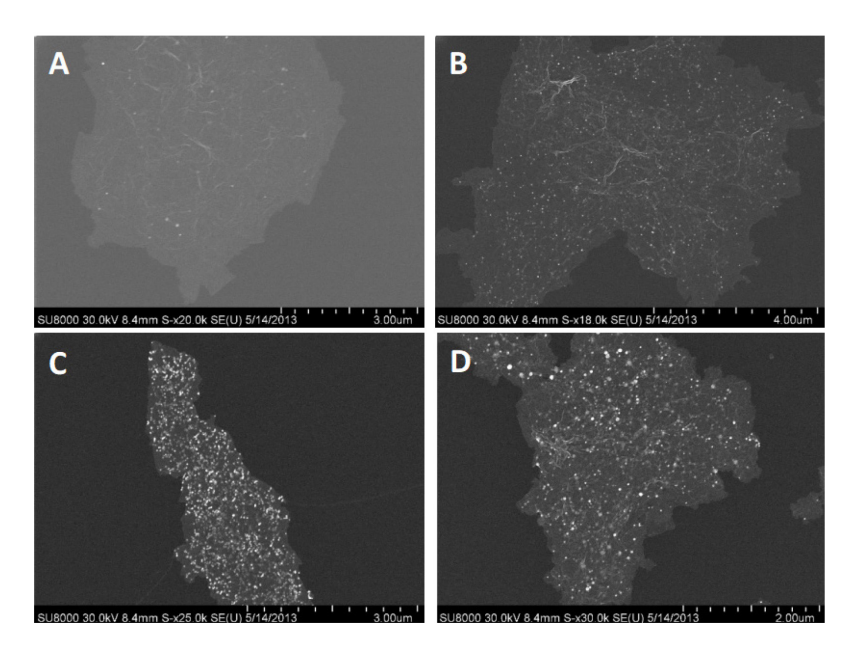


Figure 6. SEM images of the RGO/Au nanocomposites with different glucose-to-HAuCl₄ ratios. (A) 1.60/1, g/mL; (B) 0.32/1, g/mL; (C) 0.16/1, g/mL; and (D) 0.10/1, g/mL. The concentration of HAuCl₄ was 1.0 %. The amount of GO was fixed at 20.0 mg.

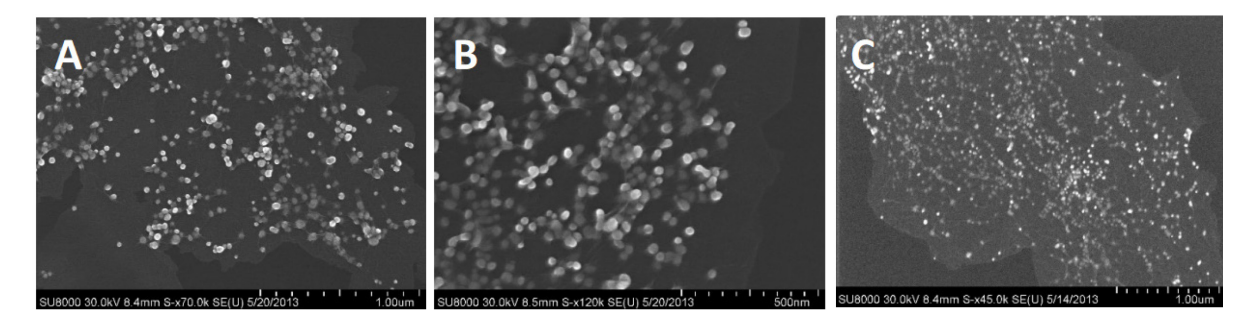


Figure 7. SEM images of the RGO/Au nanocomposites with different glucose-to-GO ratios. (A) 32/1; (B) 16/1; (C) 8/1. The amount of 1.0 % HAuCl₄ was fixed at 1.0 mL

3.3.2 Effect of glucose-to-HAuCl₄ ratio. The amount of glucose and precursor added into the reaction will certainly affect the resulting product. To better investigate their effect, we choose to study the effect of glucose-to-HAuCl₄ ratio instead of their absolute amount. With a fixed concentration of GO at 0.2 mg/mL, we adjusted the glucose-to-HAuCl₄ mass/volume ratio from 1.60/1 g/mL, 0.32/1 g/mL, 0.16/1

g/mL, to 0.10/1 g/mL during the synthetic process. The concentration of the added HAuCl₄ was 1.0%. After collecting the resulting products through centrifugation, each product was characterized with SEM. As shown in Figure 6, the size of gold nanoparticles on RGO was similar for each sample, which is around 45.3 ± 0.8 nm. However, the coverage on RGO surface increased with more HAuCl₄ addition, which was illustrated by the increased numbers of bright spots on RGO in the SEM images from Figure 5 A to C. The difference between Figure 6C and D was insignificant. Both images showed high coverage with almost every corner of RGO covered, indicating the saturation of the gold nanoparticles. The loading density of the gold nanoparticles on RGO was determined by the ratio of glucose to gold precursor. As this ratio decreased, the nanoparticle loading density increased. Because Gold nanoparticles works as the sensing spot on RGO, we believe that the highest coverage of gold nanoparticles on RGO would ensure the best performances during the electrochemical sensing. In the following experiments, the 0.16/1 (g/mL) ratio of glucose-to-HAuCl₄ composition (Figure 6C) was chosen as the optimum condition.

3.3.3 Effect of glucose-to-GO ratio. The effect of amount of glucose should also be considered from its relative amount to GO. With a fixed ratio of glucose-to-HAuCl₄ as 0.16/1 (g/mL), the effect of glucose-to-GO ratio on the final RGO/Au nanocomposite was investigated (Figure 7). We changed the glucose-to-GO mass ratio from 32/1, 16/1, to 8/1. It was found on the SEM images that the diameter of the gold nanoparticles on RGO decreased from 45.3 ± 0.8 nm to 29.5 ± 4.7 nm and 25.5 ± 0.6 nm as the glucose-to-GO ratio was decreased from 32/1 to 16/1 mg and 8/1, respectively. By fixing the concentration of HAuCl₄, increased amount of GO would provide more binding sites for gold ions to anchor. Therefore, this might decrease the diameter of single gold nanoparticles on RGO. Therefore, the particle size was determined by the ratio of glucose to GO. As this ratio decreased, the size of the gold nanoparticles on the surface of RGO also decreased.

3.4 Electrochemical Detection of L-AA, DA and UA using a RGO/Au-modified GCE as a catalyst. Accordingly, we have investigated the electrocatalytic activity of our RGO/Au nanocomposites toward oxidation of L-AA, DA and UA, followed by the simultaneous detection of these biomolecules under

physiological conditions (Figure S1 - S4). The results demonstrated the sensitive detection for these three biomolecules separately. However, the simultaneous detection of these three biomolecules were not proved yet.

3.4.1 Simultaneous determination of L-AA, DA and UA. Based on the above results for the detection of L-AA, DA and UA, the RGO/Au-GCE showed great potential for the simultaneous detection of these three biomolecules. The oxidation peak potential differences for L-AA/DA, DA/UA, and L-AA/UA were 200 mV, 150 mV, and 350 mV, respectively. Peak separations of their magnitude are generally sufficient for simultaneous analysis. Therefore, we investigated the simultaneous oxidation of the L-AA (2.2 mM), DA (160 μM) and UA (200 μM) using DPV with different electrodes. As shown in Figure 8A, bare

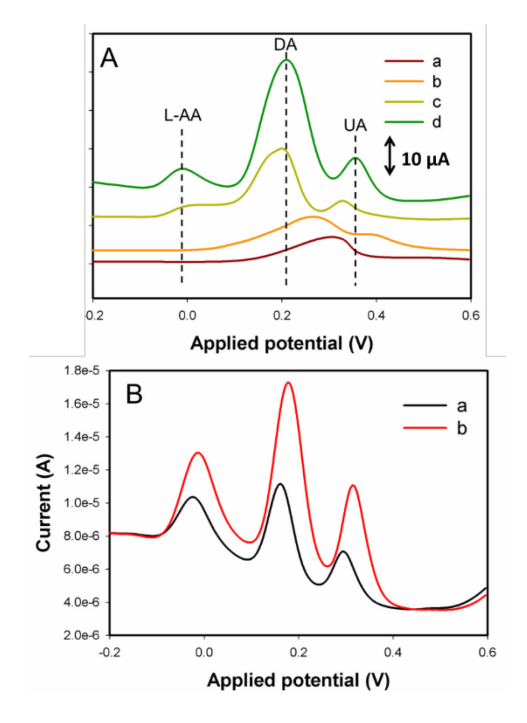


Figure 8. (A) DPV curves at bare-GCE (a), GO-GCE (b), RGO-GCE (c) and RGO/Au-GCE (d) in 0.01 M PBS (pH 7.0) containing 2.2 mM L-AA, 160 μM DA, and 200 μM UA; (B)DPVs curves at RGO/Au-GCE in 0.01 M PBS (pH 7.0) containing different concentrations of L-AA, DA and UA. (a) 0.6 mM L-AA, 10 μM DA, 20 μM UA; (b) 1.2 mM L-AA, 20 μM DA, 40 μM UA.

GCE showed only one peak that was the overlap of DA and UA. GO-GCE showed two peaks for DA and UA, which are more positive than that from RGO-GCE and RGO/Au-GCE, but still no peak for L-AA

was observed. RGO-GCE and RGO/Au-GCE were able to discriminate these three analytes. However, the peak currents for RGO/Au-GCE were higher than that of RGO-GCE, and the peak potential difference between DA and UA for RGO-GCE was smaller than that of RGO/Au-GCE. This result indicated that the Au nanoparticles and RGO all played important roles on the electrochemical catalytic activity for the simultaneous detection of L-AA, DA and UA. Two combinations of different concentrations of L-AA, DA and UA were also investigated with RGO/Au-GCE using DPV. As shown in Figure 8B, the peak currents for each molecule increased when the concentrations of these three analytes increased. Therefore, RGO/Au-GCE showed a great potential for the simultaneous detection of L-AA, DA and UA.

3.4.2 Reproducibility. Using L-AA as a model, a series of repetitive measurements were carried out in 1.0 mM L-AA solution to demonstrate the reproducibility of the RGO/Au-GCE. The results of nine measurements showed a relative standard deviation (RSD) of 3.41%, indicating excellent reproducibility for the RGO/Au-GCE. Furthermore, we found neglectable morphology and structure change of gold nanoparticles on RGO after several measurements of L-AA (Figure S5).

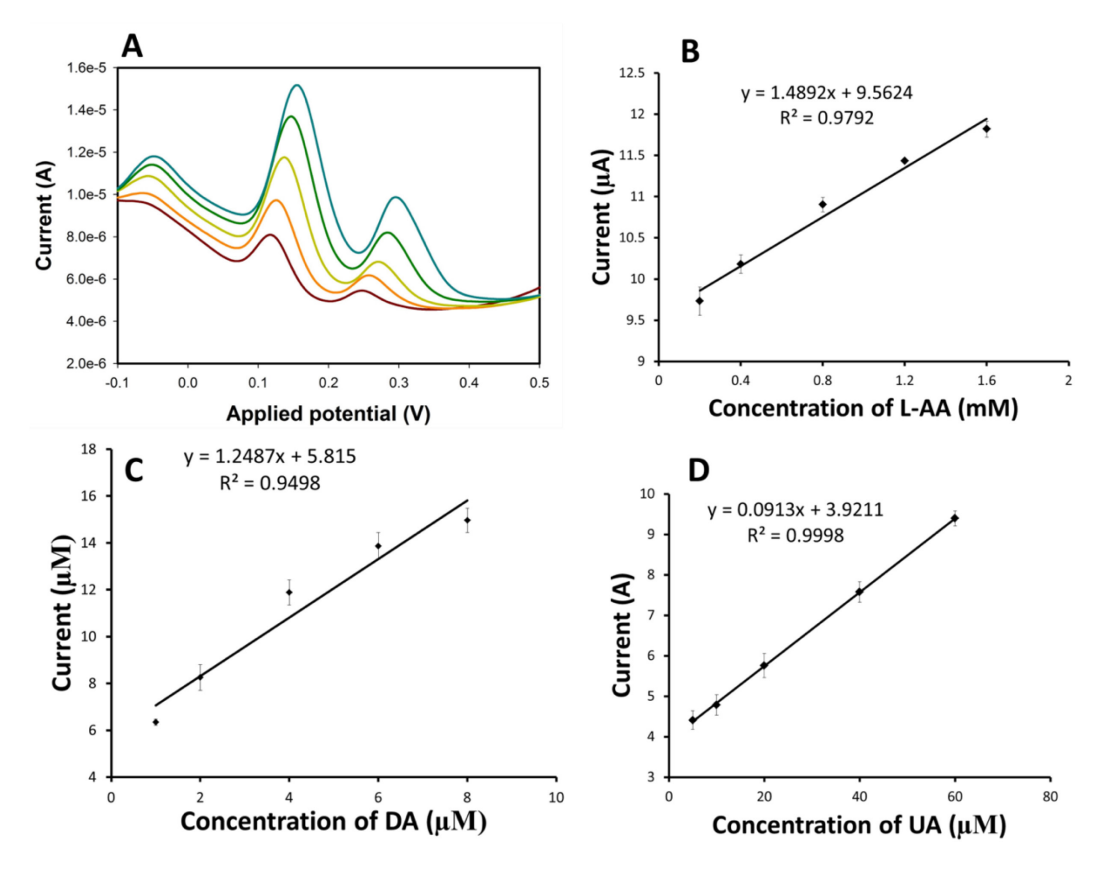


Figure 9. (A) DPV curves of the RGO/Au modified GCE in 10-times diluted serum containing individual concentration of AA, DA and UA mixture. [L-AA]: 0.2, 0.4, 0.8, 1.2, and 1.6 mM. [DA]: 1.0, 2.0, 4.0, 6.0 and 8.0 μ M. [UA]: 5.0, 10.0, 20.0, 40.0 and 60.0 μ M. The calibration curves for L-AA (B), DA (C) and UA (D) in the 10-times diluted serum.

3.4.3 Complex sample analysis. To explore the use of a RGO/Au-GCE for practical application, the electrode was used to detect the three species in fetal bovine serum samples. The fetal bovine serum was diluted 10 times with 0.01 M PBS (pH 7.0) and then spiked with certain amounts of L-AA, DA and UA. As shown in Figure 9 A, the peak currents for each analyte increased with the increased concentrations. Compared to the plot for buffer alone, the peak potential for each analyte was shifted to more negative values, which might be due to the complex matrix of the serum samples. However, for all the analytes, the RGO/Au-GCE showed a response range and high performance linear range (Figure 9B, C and D). The results indicated that the RGO/Au-GCE can be used for the sensitive simultaneous determinations of L-AA, DA and UA in the real samples.

4. Conclusion

A one-pot synthetic method was developed for the fabrication of RGO/metal (oxide) composites using glucose as the reducing agent for both GO and metal (oxide) nanoparticles. With this simple method, RGO/Au, RGO/Cu₂O, and RGO/Ag composites were easily produced. Different characterization methods successfully demonstrated the formation of RGO/metal (oxide) composite. Using RGO/Au as a model, we found that the coverage and size of gold nanoparticles on RGO were affected by the glucose-to-HAuCl₄ ratio and glucose-to-GO ratio, respectively. Furthermore, with the high electrochemical catalytic activity of RGO/Au nanocomposites, the electrochemical behaviors of L-AA, DA and UA were investigated using CV and DPV. Compared to the bare GCE, GO-GCE, and RGO-GCE, RGO/Au-GCE showed higher peak currents and larger peak potential differences for the detection of L-AA, DA and UA. Finally, the simultaneous detection of these three different analytes with high sensitivity was achieved.

ASSOCIATED CONTENT

Supporting Information. Electrochemical activity of RGO/Au GCE, detection of L-AA, DA, and UA, respectively. This material is available free of charge via the Internet at http://pubs.acs.org."

AUTHOR INFORMATION

Corresponding Author

* To whom correspondence should be addressed: Phone: 701-777-3610. Fax: 701-777-2331. E-mail: Julia.zhao@und.edu.

Notes

The authors declare no competing financial interest.

ACKNOWLEDGMENT

This work was supported by the USA National Science Foundation Grants CHE 1709160, University of North Dakota Postdoctoral Pilot Program supported by UND VPR and Art and Science College, and the North Dakota Industrial Commission Grant G-041-081.

REFERENCES

- (1) Kim, J.; Cote, L. J.; Huang, J. Two Dimensional Soft Material: New Faces of Graphene Oxide. *Acc. Chem. Res.* **2012,** *45*, 1356-1364.
- (2) Lightcap, I. V.; Kamat, P. V. Graphitic Design: Prospects of Graphene-Based Nanocomposites for Solar Energy Conversion, Storage, and Sensing. *Acc. Chem. Res.* **2012**, *46*, 2235-2243.
- (3) Chung, C.; Kim, Y.-K.; Shin, D.; Ryoo, S.-R.; Hong, B. H.; Min, D.-H. Biomedical Applications of Graphene and Graphene Oxide. *Acc. Chem. Res.* **2013**, *46*, 2211-2224.
- (4) Artiles, M. S.; Rout, C. S.; Fisher, T. S. Graphene-Based Hybrid Materials and Devices for Biosensing. *Adv. Drug. Deliv. Rev.* **2011**, *63*, 1352-1360.
- (5) Bianco, A. Graphene: Safe or Toxic? The Two Faces of the Medal. *Angew. Chem. Int. Ed.* **2013,** *52*, 4986-4997.
- (6) Georgakilas, V.; Otyepka, M.; Bourlinos, A. B.; Chandra, V.; Kim, N.; Kemp, K. C.; Hobza, P.; Zboril, R.; Kim, K. S. Functionalization of Graphene: Covalent and Non-Covalent Approaches, Derivatives and Applications. *Chem. Rev.* **2012**, *112*, 6156-6214.
- (7) Huang, X.; Qi, X.; Boey, F.; Zhang, H. Graphene-Based Composites. *Chem. Soc. Rev.* **2012**, *41*, 666-686.
- (8) Wu, D.; Zhang, F.; Liang, H.; Feng, X. Nanocomposites and Macroscopic Materials: Assembly of Chemically Modified Graphene Sheets. *Chem. Soc. Rev.* **2012**, *41*, 6160-6177.
- (9) Yoo, H.; Kim, Y.; Lee, J.; Lee, H.; Yoon, Y.; Kim, G. N-Type Reduced Graphene Oxide Field-Effect Transistors (Fets) from Photoactive Metal Oxides. *Chemistry* **2012**, *18*, 4923-4929.
- (10) Robinson, J. T.; Tabakman, S. M.; Liang, Y.; Wang, H.; Sanchez Casalongue, H.; Vinh, D.; Dai, H. Ultrasmall Reduced Graphene Oxide with High near-Infrared Absorbance for Photothermal Therapy. *J. Am. Chem. Soc.* **2011**, *133*, 6825-6831.
- (11) Jasuja, K.; Berry, V. Implantation and Growth of Dendritic Gold Nanostructures on Graphene Derivatives: Electrical Property Tailoring and Raman Enhancement. *ACS Nano* **2009**, *3*, 2358-2366.

- (12) Goncalves, G.; Marques, P. A. A. P.; Granadeiro, C. M.; Nogueira, H. I. S.; Singh, M. K.; Grácio,
- J. Surface Modification of Graphene Nanosheets with Gold Nanoparticles: The Role of Oxygen Moieties at Graphene Surface on Gold Nucleation and Growth. *Chem. Mater.* **2009**, *21*, 4796-4802.
- (13) Lightcap, I. V.; Kamat, P. V. Fortification of Cdse Quantum Dots with Graphene Oxide. Excited State Interactions and Light Energy Conversion. *J. Am. Chem. Soc.* **2012**, *134*, 7109-7116.
- (14) Yang, S.; Feng, X.; Ivanovici, S.; Müllen, K. Fabrication of Graphene-Encapsulated Oxide Nanoparticles: Towards High-Performance Anode Materials for Lithium Storage. *Angew. Chem. Int. Ed.* **2010,** *49*, 8408-8411.
- (15) Xiao, F.; Song, J.; Gao, H.; Zan, X.; Xu, R.; Duan, H. Coating Graphene Paper with 2d-Assembly of Electrocatalytic Nanoparticles: A Modular Approach toward High-Performance Flexible Electrodes. *ACS Nano* **2011**, *6*, 100-110.
- (16) Wang, C.; Li, J.; Amatore, C.; Chen, Y.; Jiang, H.; Wang, X.-M. Gold Nanoclusters and Graphene Nanocomposites for Drug Delivery and Imaging of Cancer Cells. *Angew. Chem. Int. Ed.* **2011**, *50*, 11644-11648.
- (17) Yang, K.; Feng, L.; Shi, X.; Liu, Z. Nano-Graphene in Biomedicine: Theranostic Applications. *Chem. Soc. Rev.* **2013**, *42*, 530-547.
- (18) Xu, C.; Wang, X.; Zhu, J. Graphene-Metal Particle Nanocomposites. J. Phys. Chem. C. 2008, 112, 19841-19845.
- (19) Liu, S.; Tian, J.; Wang, L.; Sun, X. A Method for the Production of Reduced Graphene Oxide Using Benzylamine as a Reducing and Stabilizing Agent and Its Subsequent Decoration with Ag Nanoparticles for Enzymeless Hydrogen Peroxide Detection. *Carbon* **2011**, *49*, 3158-3164.
- (20) Liu, S.; Wang, L.; Tian, J.; Luo, Y.; Zhang, X.; Sun, X. Aniline as a Dispersing and Stabilizing Agent for Reduced Graphene Oxide and Its Subsequent Decoration with Ag Nanoparticles for Enzymeless Hydrogen Peroxide Detection. *J. Colloid. Interface. Sci.* **2011**, *363*, 615-619.

- (21) Lu, W.; Luo, Y.; Chang, G.; Sun, X. Synthesis of Functional Sio2-Coated Graphene Oxide Nanosheets Decorated with Ag Nanoparticles for H2o2 and Glucose Detection. *Biosens. Bioelectron.* **2011**, *26*, 4791-4797.
- (22) Zhang, Y.; Liu, S.; Lu, W.; Wang, L.; Tian, J.; Sun, X. In Situ Green Synthesis of Au Nanostructures on Graphene Oxide and Their Application for Catalytic Reduction of 4-Nitrophenol. *Catal. Sci. Tech.* **2011,** *1*, 1142-1144.
- (23) Chu, Q.; Du, J.; Lu, W.; Chang, G.; Xing, Z.; Li, H.; Ge, C.; Wang, L.; Luo, Y.; Asiri, A. M.; Al-Youbi, A. O.; Sun, X. Synthesis of a Mno2 Nanosheet/Graphene Flake Composite and Its Application as a Supercapacitor Having High Rate Capability. *Chem. Plus. Chem.* **2012**, *77*, 872-876.
- (24) Liu, S.; Tian, J.; Wang, L.; Luo, Y.; Sun, X. One-Pot Synthesis of Cuo Nanoflower-Decorated Reduced Graphene Oxide and Its Application to Photocatalytic Degradation of Dyes. *Catal. Sci. Tech.* **2012**, *2*, 339-344.
- (25) Tian, J.; Liu, S.; Zhang, Y.; Li, H.; Wang, L.; Luo, Y.; Asiri, A. M.; Al-Youbi, A. O.; Sun, X. Environmentally Friendly, One-Pot Synthesis of Ag Nanoparticle-Decorated Reduced Graphene Oxide Composites and Their Application to Photocurrent Generation. *Inorg. Chem.* **2012**, *51*, 4742-4746.
- (26) Zhang, Y.; Liu, S.; Wang, L.; Qin, X.; Tian, J.; Lu, W.; Chang, G.; Sun, X. One-Pot Green Synthesis of Ag Nanoparticles-Graphene Nanocomposites and Their Applications in Sers, H₂O₂, and Glucose Sensing. *RSC Adv.* **2012**, *2*, 538-545.
- (27) Ning, R.; Tian, J.; Asiri, A. M.; Qusti, A. H.; Al-Youbi, A. O.; Sun, X. Spinel Cuco2o4 Nanoparticles Supported on N-Doped Reduced Graphene Oxide: A Highly Active and Stable Hybrid Electrocatalyst for the Oxygen Reduction Reaction. *Langmuir* **2013**, *29*, 13146-13151.
- (28) Tian, J.; Ning, R.; Liu, Q.; Asiri, A. M.; Al-Youbi, A. O.; Sun, X. Three-Dimensional Porous Supramolecular Architecture from Ultrathin G-C(3)N(4) Nanosheets and Reduced Graphene Oxide: Solution Self-Assembly Construction and Application as a Highly Efficient Metal-Free Electrocatalyst for Oxygen Reduction Reaction. *ACS Appl. Mater. Interfaces.* **2014**, *6*, 1011-1017.

- (29) Xing, Z.; Chu, Q.; Ren, X.; Ge, C.; Qusti, A. H.; Asiri, A. M.; Al-Youbi, A. O.; Sun, X. Ni3s2 Coated Zno Array for High-Performance Supercapacitors. *J. Power. Sources.* **2014**, *245*, 463-467.
- (30) Xing, Z.; Tian, J.; Asiri, A. M.; Qusti, A. H.; Al-Youbi, A. O.; Sun, X. Two-Dimensional Hybrid Mesoporous Fe₂O₃-Graphene Nanostructures: A Highly Active and Reusable Peroxidase Mimetic toward Rapid, Highly Sensitive Optical Detection of Glucose. *Biosens. Bioelectron.* **2014**, *52*, 452-457.
- (31) Lightcap, I. V.; Kosel, T. H.; Kamat, P. V. Anchoring Semiconductor and Metal Nanoparticles on a Two-Dimensional Catalyst Mat. Storing and Shuttling Electrons with Reduced Graphene Oxide. *Nano Lett* **2010**, *10*, 577-583.
- (32) Huang, J.; Zhang, L.; Chen, B.; Ji, N.; Chen, F.; Zhang, Y.; Zhang, Z. Nanocomposites of Size-Controlled Gold Nanoparticles and Graphene Oxide: Formation and Applications in Sers and Catalysis. *Nanoscale* **2010**, *2*, 2733-2738.
- (33) Liu, S.; Yan, J.; He, G.; Zhong, D.; Chen, J.; Shi, L.; Zhou, X.; Jiang, H. Layer-by-Layer Assembled Multilayer Films of Reduced Graphene Oxide/Gold Nanoparticles for the Electrochemical Detection of Dopamine. *J. Electroanal. Chem.* **2012**, *672*, 40-44.
- (34) Chen, Q.; Zhang, L.; Chen, G. Facile Preparation of Graphene-Copper Nanoparticle Composite by in Situ Chemical Reduction for Electrochemical Sensing of Carbohydrates. *Anal. Chem.* **2011**, *84*, 171-178.
- (35) Song, C.; Wu, D.; Zhang, F.; Liu, P.; Lu, Q.; Feng, X. Gemini Surfactant Assisted Synthesis of Two-Dimensional Metal Nanoparticles/Graphene Composites. *Chem. Commun.* **2012**, *48*, 2119-2121.
- (36) Wang, Y.; Yuan, R.; Chai, Y.; Yuan, Y.; Bai, L. In Situ Enzymatic Silver Enhancement Based on Functionalized Graphene Oxide and Layer-by-Layer Assembled Gold Nanoparticles for Ultrasensitive Detection of Thrombin. *Biosens. Bioelectron.* **2012**, *38*, 50-54.
- (37) Bai, S.; Shen, X.; Zhu, G.; Li, M.; Xi, H.; Chen, K. In Situ Growth of Ni(X)Co(100-X) Nanoparticles on Reduced Graphene Oxide Nanosheets and Their Magnetic and Catalytic Properties. *ACS Appl. Mater. Interfaces.* **2012**, *4*, 2378-2386.

- (38) Zhou, X.; Huang, X.; Qi, X.; Wu, S.; Xue, C.; Boey, F. Y. C.; Yan, Q.; Chen, P.; Zhang, H. In Situ Synthesis of Metal Nanoparticles on Single-Layer Graphene Oxide and Reduced Graphene Oxide Surfaces. *J. Phys. Chem. C.* **2009**, *113*, 10842-10846.
- (39) Iliut, M.; Leordean, C.; Canpean, V.; Teodorescu, C. M.; Astilean, S. A New Green, Ascorbic Acid-Assisted Method for Versatile Synthesis of Au-Graphene Hybrids as Efficient Surface-Enhanced Raman Scattering Platforms. *J. Mater. Chem. C.* **2013**. *1*, 4094-4104.
- (40) Kim, Y. K.; Han, S. W.; Min, D. H. Graphene Oxide Sheath on Ag Nanoparticle/Graphene Hybrid Films as an Antioxidative Coating and Enhancer of Surface-Enhanced Raman Scattering. *ACS Appl. Mater. Interfaces.* **2012**, *4*, 6545-6551.
- (41) Ren, W.; Fang, Y.; Wang, E. A Binary Functional Substrate for Enrichment and Ultrasensitive Sers Spectroscopic Detection of Folic Acid Using Graphene Oxide/Ag Nanoparticle Hybrids. *ACS Nano* **2011**, *5*, 6425-6433.
- (42) Xu, S.; Yong, L.; Wu, P. One-Pot, Green, Rapid Synthesis of Flowerlike Gold Nanoparticles/Reduced Graphene Oxide Composite with Regenerated Silk Fibroin as Efficient Oxygen Reduction Electrocatalysts. *ACS Appl. Mater. Interfaces.* **2013**, *5*, 654-662.
- (43) Zhu, C.; Guo, S.; Fang, Y.; Dong, S. Reducing Sugar: New Functional Molecules for the Green Synthesis of Graphene Nanosheets. *ACS Nano* **2010**, *4*, 2429-2437.
- (44) Zhang, Z.; Chen, H.; Xing, C.; Guo, M.; Xu, F.; Wang, X.; Gruber, H.; Zhang, B.; Tang, J. Sodium Citrate: A Universal Reducing Agent for Reduction / Decoration of Graphene Oxide with Au Nanoparticles. *Nano. Res.* **2011**, *4*, 599-611.
- (45) Li, Y.; Gao, W.; Ci, L.; Wang, C.; Ajayan, P. M. Catalytic Performance of Pt Nanoparticles on Reduced Graphene Oxide for Methanol Electro-Oxidation. *Carbon* **2010**, *48*, 1124-1130.
- (46) Dong, X.; Huang, W.; Chen, P. In Situ Synthesis of Reduced Graphene Oxide and Gold Nanocomposites for Nanoelectronics and Biosensing. *Nanoscale. Res. Lett.* **2010**, *6*, 60.

- (47) Kalimuthu, P.; John, S. A. Electropolymerized Film of Functionalized Thiadiazole on Glassy Carbon Electrode for the Simultaneous Determination of Ascorbic Acid, Dopamine and Uric Acid. *Bioelectrochemistry* **2009**, *77*, 13-18.
- (48) Zen, J.-M.; Chen, P.-J. A Selective Voltammetric Method for Uric Acid and Dopamine Detection Using Clay-Modified Electrodes. *Anal. Chem.* **1997**, *69*, 5087-5093.
- (49) Randrup, A. Role of Brain Dopamine in the Antipsychotic Effect of Neuroleptics. Evidence from Studies of Amphetamine-Neuroleptic Interaction. *Mod. Probl. Pharmacopsychiatry.* **1970,** *5*, 60-65.
- (50) Fraga, C. G.; Motchnik, P. A.; Shigenaga, M. K.; Helbock, H. J.; Jacob, R. A.; Ames, B. N. Ascorbic Acid Protects against Endogenous Oxidative DNA Damage in Human Sperm. *Proc. Natl. Acad. Sci. U. S. A.* **1991,** 88, 11003-11006.
- (51) Hare, J. M.; Johnson, R. J. Uric Acid Predicts Clinical Outcomes in Heart Failure: Insights Regarding the Role of Xanthine Oxidase and Uric Acid in Disease Pathophysiology. *Circulation* **2003**, *107*, 1951-1953.
- (52) Sheng, Z.-H.; Zheng, X.-Q.; Xu, J.-Y.; Bao, W.-J.; Wang, F.-B.; Xia, X.-H. Electrochemical Sensor Based on Nitrogen Doped Graphene: Simultaneous Determination of Ascorbic Acid, Dopamine and Uric Acid. *Biosens. Bioelectron.* **2012**, *34*, 125-131.
- (53) Li, S.-M.; Yang, S.-Y.; Wang, Y.-S.; Lien, C.-H.; Tien, H.-W.; Hsiao, S.-T.; Liao, W.-H.; Tsai, H.-P.; Chang, C.-L.; Ma, C.-C. M.; Hu, C.-C. Controllable Synthesis of Nitrogen-Doped Graphene and Its Effect on the Simultaneous Electrochemical Determination of Ascorbic Acid, Dopamine, and Uric Acid. *Carbon* **2013**, *59*, 418-429.
- (54) Han, D.; Han, T.; Shan, C.; Ivaska, A.; Niu, L. Simultaneous Determination of Ascorbic Acid, Dopamine and Uric Acid with Chitosan-Graphene Modified Electrode. *Electroanalysis* **2010**, *22*, 2001-2008.

- (55) Sun, C.-L.; Chang, C.-T.; Lee, H.-H.; Zhou, J.; Wang, J.; Sham, T.-K.; Pong, W.-F. Microwave-Assisted Synthesis of a Core–Shell Mwcnt/Gonr Heterostructure for the Electrochemical Detection of Ascorbic Acid, Dopamine, and Uric Acid. *ACS Nano* **2011**, *5*, 7788-7795.
- (56) Zhang, L.; Jiang, X. Attachment of Gold Nanoparticles to Glassy Carbon Electrode and Its Application for the Voltammetric Resolution of Ascorbic Acid and Dopamine. *J. Electroanal. Chem.* **2005**, *583*, 292-299.
- (57) Hu, G.; Ma, Y.; Guo, Y.; Shao, S. Electrocatalytic Oxidation and Simultaneous Determination of Uric Acid and Ascorbic Acid on the Gold Nanoparticles-Modified Glassy Carbon Electrode. *Electrochimica*. *Acta*. **2008**, *53*, 6610-6615.
- (58) Zhang, J.; Yang, H.; Shen, G.; Cheng, P.; Zhang, J.; Guo, S. Reduction of Graphene Oxide Via L-Ascorbic Acid. *Chem. Commun.* **2010**, *46*, 1112-1114.
- (59) Raveendran, P.; Fu, J.; Wallen, S. L. A Simple and "Green" Method for the Synthesis of Au, Ag, and Au-Ag Alloy Nanoparticles. *Green. Chem.* **2006**, *8*, 34-38.

Table of Contents

